

Cell geometry designs for efficient plasma display panels

G. Veronis and U. S. Inan^{a)}

Space, Telecommunications, and Radioscience Laboratory, Stanford University, Stanford, California 94305

(Received 1 April 2002; accepted 6 August 2002)

We investigate the performance of several nonstandard plasma display panel cell geometry designs involving two-dimensional variations of the standard coplanar-electrode design. A cell design with a modified shape of sustain electrodes is found to have $\sim 20\%$ larger visible light generation efficiency without substantial increase of the operating voltages. Similar performance improvement is achieved by designs with different shapes of the upper dielectric, or by those involving two different dielectric layers. The dependence of cell performance on the design parameters of these structures is investigated. © 2002 American Institute of Physics. [DOI: 10.1063/1.1511272]

I. INTRODUCTION

Plasma display panels (PDPs) are one of the leading candidates in the competition for large-size, high-brightness, high-contrast-ratio flat panel displays, suitable for high definition television (HDTV) wall-mounted monitors.^{1,2} Their advantages are high resolution, wide viewing angle, low weight, and simple manufacturing process for fabrication. Recent progress of PDP technology development and manufacturing has been remarkable.^{3,4} However, there are still problems that need to be resolved to popularize the PDP as a home commodity. One of the most critical issues in ongoing PDP research is the improvement of the luminous efficiency, which is still low compared to conventional cathode ray tube displays. Another important problem is the relatively high operating voltages.

PDP cells are small (cell height is $\sim 150 \mu\text{m}$) and provide limited access for diagnostic measurements. As a result, experimental studies of the transient plasma discharges in PDPs are extremely difficult, and computer-based modeling is currently essential for understanding PDP physics and optimizing its operation. Computer simulations are effective in identifying the basic properties of the discharge dynamics and the dominant mechanisms of light emission. In addition, simulation models are usually successful in predicting the effects on the performance of the device of variations in design parameters, such as cell geometry, applied voltage waveforms, and gas mixture. Although simulation results are usually in qualitative rather than quantitative agreement with experimental display measurements, they are used very effectively to provide directions for future PDP design.

Typical color plasma displays consist of two glass plates, each with parallel electrodes deposited on their surfaces. The electrodes are covered with a dielectric film. The plates are sealed together with their electrodes at right angles, and the gap between the plates is first evacuated and then filled with an inert gas mixture. A protective MgO layer is deposited above the dielectric film. The primary role of this layer is to decrease the breakdown voltage due to the high secondary-electron emission coefficient of MgO. The UV photons emitted by the discharge hit the phosphors deposited on the walls

of the PDP cell and are converted into visible photons. Each cell contains a specific type of phosphor that emits one primary color, red, green, or blue.

The most common type of color plasma display is the coplanar-electrode PDP. In this PDP type, each cell is formed by the intersection of a pair of transparent sustain electrodes on the front plate, and an address electrode on the back plate. During operation, a periodic voltage with a frequency of 50–350 kHz is continuously applied between each pair of sustain electrodes. The amplitude of the sustain voltage is below the breakdown voltage. A cell is turned ON by applying a write voltage pulse between the address electrode and one of the sustain electrodes. The discharge which is initiated results in the deposition of surface charge on the dielectric layers covering these two electrodes. The superposition of the electric field induced by the deposited surface charge and of the electric field of the applied sustaining voltage results in the ignition of sustain discharges between the pair of sustain electrodes.

Several alternative designs have previously been proposed as a way to increase the luminous efficiency of the PDP. These designs modified the arrangement of individual cells of the display or the three-dimensional structure of the electrodes.^{4,5} Other methods were based on rf discharge⁶ or a different mixture composition.⁷ However, the effect of simpler two-dimensional variations of the PDP cell geometry on the performance of the device has not been investigated in detail, although some two-dimensional variations have been proposed.^{8,9} In this article, we consider several nonstandard cell geometry designs and investigate in detail the effect of variations of the cell geometry design on the operating voltages and the efficiency of the device. The alternative cell designs are variations of the standard coplanar-electrode cell design used in most PDPs. In addition, we put forth new cell structures that result in optimum device performance and evaluate the dependence of PDP performance on the design parameters of these structures. We use a two-dimensional (2D) self-consistent model to simulate the microdischarges in PDP cells, which is briefly described in Sec. II. The results obtained using this model for the various cell geometry designs are presented in Sec. III, while our conclusions are summarized in Sec. IV.

^{a)}Electronic mail: inan@nova.stanford.edu

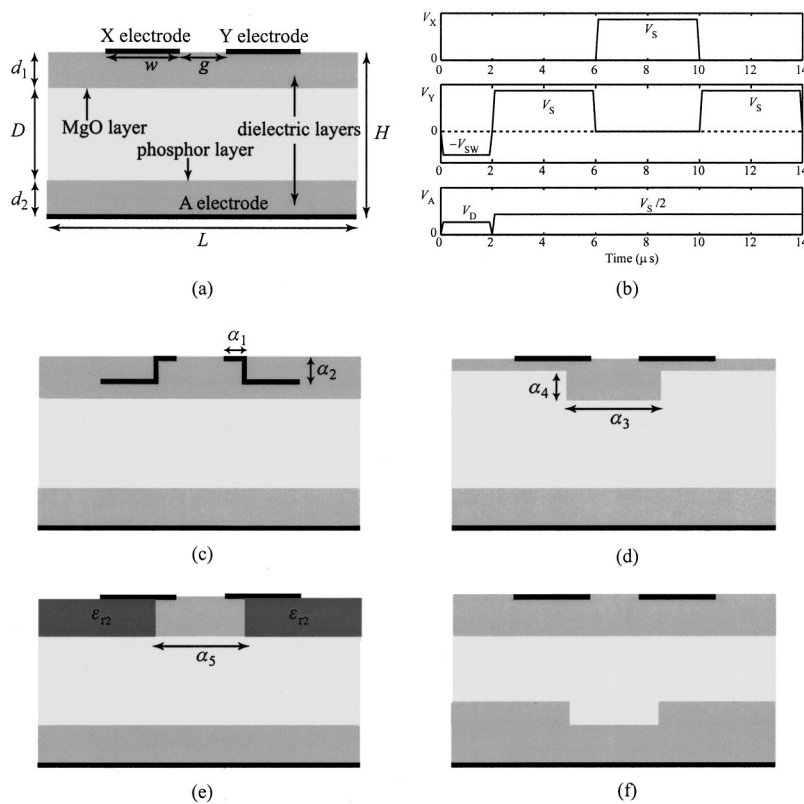


FIG. 1. (a) Schematic of the standard coplanar-electrode plasma display panel (PDP) cell. (b) Driving scheme used in the simulations showing the voltage applied to the X, Y, and A electrodes. Initially, $2 \mu\text{s}$ address pulses are applied, followed by a sequence of alternating polarity sustain pulses. The sustaining frequency is 125 kHz. The address electrode is biased to a voltage of $V_s/2$ during the sustaining phase. (c) Schematic of the electrode-shaping geometry. (d) Schematic of the dielectric-shaping geometry. (e) Schematic of a geometry design involving two different dielectric layers. (f) Schematic of a geometry design with modified shape of the lower dielectric layer.

II. MODEL DESCRIPTION

We provide only a brief description of the self-consistent fluid model used to simulate the microdischarges in the PDP cell, since this model has been described in detail elsewhere.¹⁰

The continuity equations are solved for electrons, atomic (Ne^+ , Xe^+) and molecular (Ne_2^+ , Xe_2^+ , NeXe^+) ions, and excited species [Ne_m^* , $\text{Xe}^*(^3\text{P}_1)$, $\text{Xe}^*(^3\text{P}_2)$, Xe^{**} , $\text{Xe}_2^*(\text{O}_u^+)$, $\text{Xe}_2^*(^3\Sigma_u^+)$, $\text{Xe}_2^*(^1\Sigma_u^+)$] for a Ne–Xe mixture. We use the drift–diffusion equation as an approximation to the momentum equation. The electric field within the cell is self-consistently calculated by solving Poisson’s equation. Electron impact reaction rates and transport coefficients are assumed to be functions of the electron mean energy which is determined by solving the electron energy equation. We use a finite difference method to solve the system of partial differential equations. The continuity equations and the electron energy equation are solved implicitly, while semi-implicit methods are used for the integration of the coupled continuity and field equations, and for the source term in the electron energy equation. The electron impact ionization and excitation frequencies as well as the electron mobility are calculated using the Boltzmann code ELENDF.¹¹ Electron–atom collision cross sections for Ne and Xe are taken from the SIGLO series.¹² Rate coefficients for Penning ionization, dimer ions formation, charge exchange, recombination, and neutral kinetics reactions, as well as excited species lifetimes are taken from Ref. 13.

In order to calculate the visible light output of the PDP cell, we implement a radiation transport model, similar to the one described in Ref. 14. The source functions for UV pho-

tons are computed by the plasma dynamics fluid model. We assume that UV photons are emitted isotropically, and calculate their fluxes on the phosphor surface using ray-tracing techniques. A unity UV-to-visible conversion efficiency is assumed for the phosphor. The fluxes of visible photons on the output window are also calculated using ray-tracing techniques, assuming Lambertian emission from the phosphor surface.

III. RESULTS

The geometry of the standard coplanar-electrode PDP cell used in the simulations is shown in Fig. 1(a). The cell consists of two sustain electrodes, X and Y, separated from the gas by a dielectric layer. An MgO layer is deposited on the dielectric film. The bottom of the cell consists of the address electrode A separated from the gas by a dielectric layer with a phosphor layer on top. The output window of the device is supposed to be the top side of the upper dielectric layer, noting that the sustain electrodes are transparent. In all cases, the gas mixture filling the region between the dielectrics is a Xe–Ne mixture with 4% Xe at a pressure of 500 Torr. The height and width of the cell are $H=210 \mu\text{m}$ and $L=1260 \mu\text{m}$, respectively. Our reference case is characterized by the parameter values $g=100 \mu\text{m}$, $w=300 \mu\text{m}$, $d_1=30 \mu\text{m}$, $d_2=30 \mu\text{m}$, and $\epsilon_r=10$, where g is the electrode gap length, w is the sustain electrode width, d_1, d_2 are the lengths of the upper and lower dielectric layers, respectively, and ϵ_r is the dielectric constant. This reference case was one of the cases considered in Veronis and Inan.¹⁰

The voltages applied to the three electrodes during the simulation are shown in Fig. 1(b). Initially, a data pulse V_D

and a base-write pulse $-V_{SW}$ are applied simultaneously to the *A* and *Y* electrodes, respectively. These are followed by a sequence of alternating sustaining voltage pulses V_S between the two sustain electrodes *X* and *Y*. During the sustain phase, the address electrode *A* is biased to a voltage of $V_S/2$ to prevent undesired discharges between the address electrode and the sustain electrodes. The frequency of the sustaining waveform is 125 kHz and the rise and fall times of all pulses are 100 ns. The duration of the address pulses is 2 μ s.

A. Calculation of voltage margin and visible light generation efficiency

As in Veronis and Inan,¹⁰ we focus our attention on the operating voltages and the visible light generation efficiency of the PDP cell. PDP cells can operate only if the applied sustaining voltage is held within certain limits. The initial address pulse triggers a discharge between the *A* and *Y* electrodes. This discharge is quenched by surface charges accumulated on the dielectrics. Subsequent sustain discharges occur only in the addressed cells, since the sustaining voltage V_S is below the breakdown voltage, as discussed above. The minimum sustaining voltage V_{Smin} is defined as the minimum value of V_S which leads to a steady sequence of sustaining discharges in an addressed cell.¹⁵ The firing voltage V_f is defined as the breakdown voltage in an unaddressed cell. The sustaining voltage V_S must at all times be less than V_f in order to avoid discharges in cells which are not addressed. V_{Smin} and V_f define the voltage margin of the cell. In real PDPs, these voltages exhibit some statistical variation, since cells have slightly different dimensions.¹⁵ The voltage margin of the cell should therefore be as large as possible to ensure reliable operation of the display.

In our studies, we investigate the effect of cell geometry design on the numerical values of V_{Smin} and V_f . The calculation of V_{Smin} and V_f is done as in Veronis and Inan¹⁰ and is repeated here for completeness. For the calculation of V_f , a sustain pulse V_S is applied to one of the sustain electrodes and *A* is biased to $V_S/2$, as described above. We use the full 2D model to iteratively calculate (to within an accuracy of 1 V) the minimum voltage V_f which leads to breakdown. In all cases, the breakdown occurs between the two sustain electrodes.

For the calculation of V_{Smin} , we first apply the address pulses V_D and $-V_{SW}$ described above. In all cases, we use $V_{SW}=150$ V, and for the reference case $V_D=80$ V. In all other cases, V_D is chosen so that the breakdown parameter¹⁶ $\mu = (\alpha_{Ne}\gamma_{Ne} + \alpha_{Xe}\gamma_{Xe})[e^{(\alpha_{Ne} + \alpha_{Xe})D} - 1]/(\alpha_{Ne} + \alpha_{Xe})$ is constant, where α_{Ne} and α_{Xe} are the partial first Townsend ionization coefficients for Ne and Xe, respectively, γ_{Ne} and γ_{Xe} are the secondary-electron emission coefficients for Ne and Xe ions, respectively, on MgO, and D is the discharge gap length [Fig. 1(a)]. In cases of nonconstant discharge gap length [e.g., Fig. 1(d)], we use the minimum value of the gap length. A sequence of sustaining pulses V_S is then applied between the sustain electrodes [Fig. 1(b)]. We once again use the full 2D model (in an iterative fashion) to calculate (to within an accuracy of 1 V) the minimum voltage V_{Smin} which leads to a steady sequence of sustain discharges. In

other words, we lower the sustain voltage until the discharge distinguishes.

The UV photons which excite the phosphors are emitted by certain excited states of Xe [$Xe^*(^3P_1)$ (resonant state) at 147 nm, $Xe_2^*(O_u^+)$ at 150 nm, $Xe_2^*(^3\Sigma_u^+)$ and $Xe_2^*(^1\Sigma_u^+)$ at 173 nm (excimer states)].¹³ The excited phosphors in turn emit visible photons. We define the visible light generation efficiency of the cell as the ratio of total visible photon energy which reaches the output window to the total energy dissipated during a sustaining period ($T=8$ μ s)

$$\eta = \frac{\int_T dt \int_{S_{out}} ds \Gamma_{ph} \epsilon_{ph}}{\int_T dt \int_V dv (\mathbf{J}_e + \sum_{i=1}^{N_{ion}} \mathbf{J}_{ioni}) \cdot \mathbf{E}}, \quad (1)$$

where Γ_{ph} is the number of visible photons reaching the output window per unit area and per unit time, ϵ_{ph} is the visible photon energy, \mathbf{J}_e and \mathbf{J}_{ioni} are the electronic and ionic current (of ion *i*) respectively, and \mathbf{E} is the electric field. We assume that the visible photon wavelength is 550 nm.

For the calculation of efficiency, the voltage waveform shown in Fig. 1(b) is applied in all cases to the cell electrodes. As in Veronis and Inan,¹⁰ the sustaining voltage is chosen to be the midmargin voltage, defined as $V_{Sm} = (V_{Smin} + V_f)/2$. The midmargin voltage is usually chosen as the point of operation of the PDP to ensure reliability. We calculate the efficiency of the PDP cell in the periodic steady state, typically involving the application of at least five sustaining pulses.

B. Electrode-shaping geometry

In the standard coplanar-electrode geometry, there is a trade off between high light generation efficiency and low operating voltages.¹⁰ In Fig. 2, we show the effect of the variation of the sustain electrode gap length *g* [Fig. 1(a)] on the visible light generation efficiency η and the midmargin voltage V_{Sm} of the PDP cell. We observe that larger values of *g* result in larger values of both η and V_{Sm} . Similarly, larger values of the length of the upper dielectric d_1 [Fig. 1(a)] result in larger values of both η and V_{Sm} .

Figure 2 also shows the visible light generation efficiency η and midmargin voltage V_{Sm} for alternative cell geometry designs. In Fig. 1(c) we show a PDP cell geometry with modified shape of sustain electrodes which for brevity will heretofore be referred to as the electrode-shaping geometry. This design is characterized by the design parameters a_1 and a_2 . Fig. 2 shows η and V_{Sm} for this electrode-shaping geometry with $a_1=100$ μ m and $a_2=22.5$ μ m, all other parameters being the same as in the reference case. We observe that the midmargin voltage V_{Sm} is essentially the same as in the reference case, while the visible light generation efficiency η increases by $\sim 16\%$. If a_1 and a_2 are kept constant, and the sustain electrode width *w* is increased from 300 to 400 μ m, the increase in the visible light generation efficiency η with respect to the reference case is found to be $\sim 20\%$, while the operating voltage increases by only a few volts. It should be noted that the substantial increase in η for the electrode-shaping geometry, when *w* is increased, is not observed in the standard coplanar-electrode geometry, as

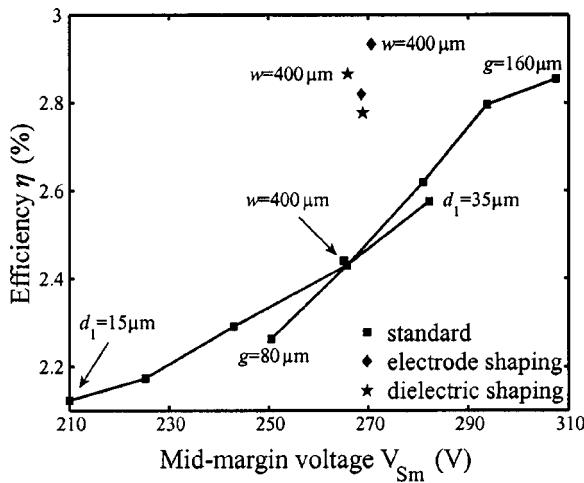


FIG. 2. Visible light generation efficiency η and midmargin voltage V_{Sm} of various cell geometry designs. Results are shown for the standard coplanar-electrode, the electrode-shaping, and the dielectric-shaping geometries. The effect of the variation of the sustain electrode gap length g and of the upper dielectric layer length d_1 is shown for the standard geometry. All other cell parameters are the same as in the reference case. Note that the reference case corresponds to the intersection point of the two curves.

shown in Fig. 2. It should also be noted that for a given cell width L the sustain electrode width w has to be small enough to ensure that no undesired discharges occur with sustain electrodes of adjacent cells. Thus, there is a limit to the increase in efficiency that can be achieved in the electrode-shaping geometry by increasing w .

It is obvious from the results presented in Fig. 2 that the electrode-shaping geometry has a better performance than the standard coplanar-electrode geometry of Fig. 1(a). It results in an increase in visible light generation efficiency without a substantial increase of the operating voltages. The operating voltages remain the same because the structure in the middle of the cell is the same in both the standard coplanar-electrode and electrode-shaping geometries. Figures 3(a) and 3(b) show equipotential lines for the standard and the electrode-shaping geometries, respectively. We observe that in both cases the electric field in the gap is maximum in the region between the two sustain electrodes in the cell center. As the applied voltage is increased, the breakdown condition first occurs in discharge paths in this high-field region. We observe that the electric field structure is the same for both designs in the high-field region and that the breakdown voltage is therefore not significantly different. In other words, the different shape of sustaining electrodes of the new structure does not significantly perturb the electric field distribution in the region where breakdown first occurs.

In order to better understand the reasons for the increase in the visible light generation efficiency, we focus our attention on the excitation efficiency. The visible light generation efficiency defined in Eq. (1) can also be written as

$$\begin{aligned} \eta &= \eta_1 \eta_2 \eta_3 \eta_4, \\ \eta_1 &= \epsilon_{el} / (\epsilon_{el} + \epsilon_{ion}), \\ \eta_2 &= \epsilon_{exc} / \epsilon_{el}, \\ \eta_3 &= \epsilon_{UV} / \epsilon_{exc}, \\ \eta_4 &= \epsilon_{vis} / \epsilon_{UV}, \end{aligned} \tag{2}$$

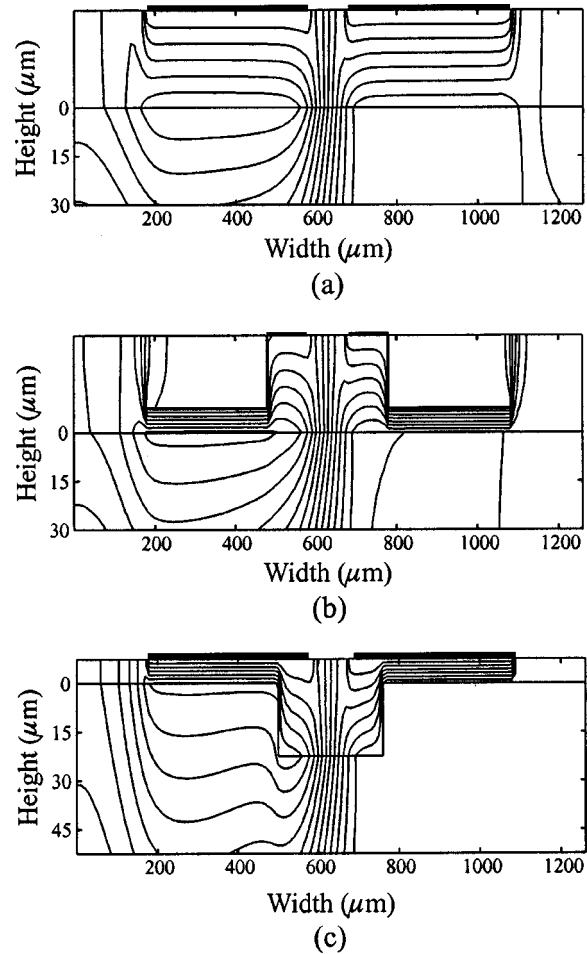


FIG. 3. (a)–(c) Equipotential lines for the standard, the electrode-shaping, and the dielectric-shaping geometries, respectively, at the end of a sustaining period ($t=18 \mu s$). The increment between the contours is 20 V.

where ϵ_{el} and ϵ_{ion} are the total energies dissipated per period by electrons and ions, respectively, ϵ_{exc} is the total energy lost by electrons per period in collisions that lead to the production of UV emitting excited states of xenon, ϵ_{UV} is the total UV emitted energy per period, and ϵ_{vis} is the total visible light energy reaching the output window. Physically, η_1 is the efficiency of the discharge in heating the electrons, η_2 is the efficiency of electrons in producing UV emitting states of xenon, and η_3 is the efficiency of emission of UV photons by xenon excited atoms and molecules. Finally, η_4 is an additional factor in the overall visible light generation efficiency η , related to the efficiency of transport of UV photons to the phosphor layer and of the visible photons to the output window, and to the UV-to-visible conversion efficiency of the phosphor. Our analyses indicate that the effect of cell geometry variations on η_3 is small, because the rates of the reactions that lead to emission of UV photons from xenon excited states are solely determined by the gas mixture composition. Similarly, the effect of cell geometry variations on η_4 is small. Although we might expect that geometry variations could result in UV emission closer to the phosphor layer, and therefore higher η_4 , the increase in η_4 is relatively small for the 2D cell geometry variations considered herein. We therefore focus our attention on the excitation efficiency defined as $\eta_{exc} = \eta_1 \eta_2$ representing the components of the

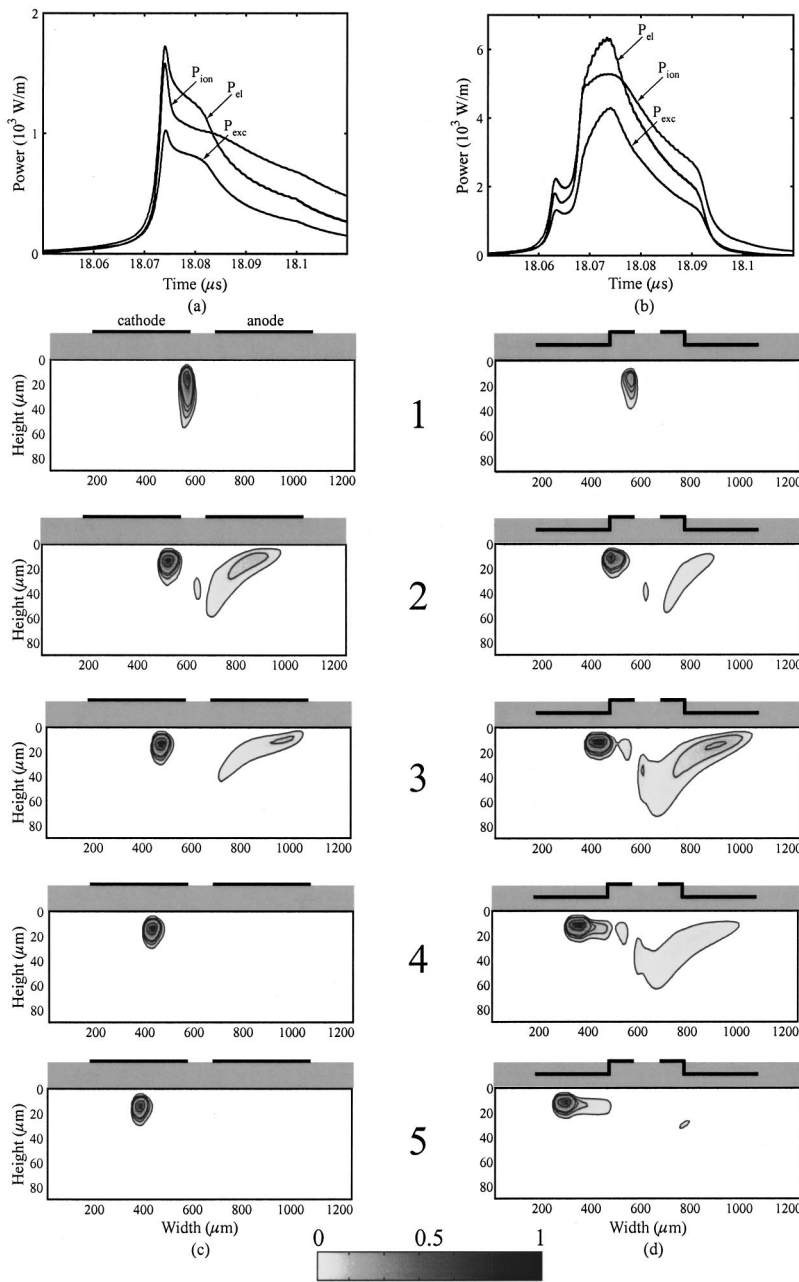


FIG. 4. (a) and (b) Dissipated ion power P_{ion} , dissipated electron power P_{el} , and power spent on Xe excitation P_{exc} per unit length for the standard and electrode-shaping geometries, respectively. (c) and (d) Normalized power spent for xenon excitation, integrated over 5 ns consecutive time intervals, for the standard and electrode-shaping geometries, respectively. The starting time for integration is 75 ns and 70 ns after the beginning of a sustaining period for the standard and electrode-shaping geometries, respectively. The maximum in the gray scale corresponds to $1.73 \times 10^7 \text{ m}^{-2}$. The contours correspond to 0.05, 0.1, 0.15, 0.2, 0.5, and 0.8 of the maximum value. Note the different vertical scale in each plot. In all cases, height is measured from the MgO layer surface.

overall efficiency most significantly affected by geometry variations. The excitation efficiency is therefore given by

$$\eta_{exc} = \frac{\int_T dt \int_V dv \sum_{i=1}^{N_{exc}} n_e v_i^* \epsilon_{exci}}{\int_T dt \int_V dv (\mathbf{J}_e + \sum_{i=1}^{N_{ion}} \mathbf{J}_{ioni}) \cdot \mathbf{E}}, \quad (3)$$

where n_e is the electron density, v_i^* is the excitation frequency of excited state of Xe i which leads through a series of reactions to UV photon production, and ϵ_{exci} is the corresponding electron loss energy.

In Figs. 4(a) and 4(b), we show the dissipated ion power, dissipated electron power, and power spent on Xe excitation in the PDP cell per unit length of the standard [Fig. 1(a)] and electrode-shaping [Fig. 1(c)] geometries, respectively. Results are shown as a function of time, during the discharge caused by the fifth sustain pulse applied to the Y electrode starting at $t = 18 \mu\text{s}$. We observe that the duration of the

discharge is shorter for the electrode-shaping geometry and that the peak power dissipation is higher by almost a factor of 3.

We may note that the excitation efficiency can also be written as¹⁰

$$\eta_{exc} = \int_V dv \left[\int_T dt \frac{p_{exc}}{\epsilon_{tot}} \right], \quad (4)$$

where $p_{exc} = \sum_{i=1}^{N_{exc}} n_e v_i^* \epsilon_{exci}$, and $\epsilon_{tot} = \int_T dt \int_V dv p$, where $p = (\mathbf{J}_e + \sum_{i=1}^{N_{ion}} \mathbf{J}_{ioni}) \cdot \mathbf{E}$. Equation (4) suggests that the excitation efficiency η_{exc} is obtained by integrating (over space and time) the power spent for xenon excitation (p_{exc}) normalized by the total energy dissipated in the discharge (ϵ_{tot}). For purposes of brevity, this quantity, which is directly related to the excitation efficiency, will heretofore be referred to as the normalized power spent for xenon excitation. In

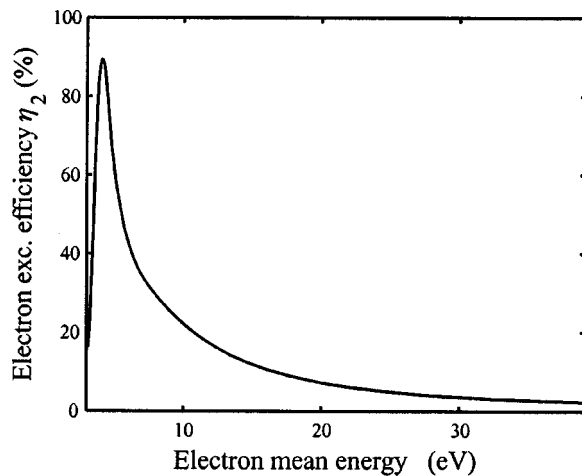


FIG. 5. The electron excitation efficiency η_2 as a function of the electron mean energy.

Figs. 4(c) and 4(d), we show the normalized power spent for xenon excitation, integrated over 5 ns time intervals, for the standard [Fig. 1(a)] and electrode-shaping [Fig. 1(c)] geometries, respectively. We observe that high excitation occurs both in the cathode sheath–plasma interface and in the bulk plasma regions.¹⁷ The bulk plasma excitation region is wider in the electrode-shaping geometry [snapshots 2, 3, and 4 of Figs. 4(c) and 4(d)], for which the outer ends of the sustain electrodes are closer to the gap [Fig. 1(c)] so that the electric field is enhanced in the corresponding gap region. Due to the enhancement of the electric field in the outer parts of the gap, wider discharge paths become increasingly favorable in this structure. We note that wider plasma region results in higher discharge efficiency. The cathode ion sheath region is characterized by high electric fields and high electron temperatures, while the bulk plasma region is characterized by much lower electric fields and consequently lower electron temperatures. In Fig. 5, we show η_2 as a function of electron mean energy, in constant uniform electric fields, obtained using ELENDF.¹¹ We observe that η_2 is maximized at ~ 4 eV. Our analyses indicate that, during the discharge, the electric field is high enough to sustain electron temperatures above this threshold in all regions of significant excitation. Excitation efficiency is therefore a decreasing function of electron temperature for PDP discharge conditions. It is for this reason that the bulk plasma region of the discharge is more efficient than the sheath region, and that wider plasma region results in higher efficiency. In addition, we observe that the bulk plasma region in the electrode-shaping geometry is more efficient than the bulk plasma region of the standard structure [snapshots 2 and 3 of Figs. 4(c) and 4(d)], due to lower electric fields and consequently lower electron temperatures in the bulk plasma region. Finally, we observe that the cathode sheath region is also more efficient in the electrode-shaping design [snapshots 4 and 5 of Figs. 4(c) and 4(d)]. Excitation is more confined in the cathode region of the standard structure. As mentioned above, the electric field is higher in the outer part of the gap in the electrode-shaping geometry. Electron temperatures are therefore higher and η_2 is lower. However, the excitation region in the cathode ion

sheath for the electrode-shaping geometry includes a “tail” region [snapshots 4 and 5 of Fig. 4(d)] so that the cathode region is overall more efficient for this new structure. We found that the tail excitation region is due to longer discharge duration in individual discharge paths in the electrode-shaping geometry, because it takes more time to produce (via ionization) the charge required to quench the discharge. For example, in the case presented in Fig. 4, the distance of the outer part of the sustain electrodes from the gap for the electrode-shaping design is $7.5 \mu\text{m}$, while that for the standard design is $30 \mu\text{m}$. The equivalent capacitance and therefore the charge required to quench the discharge is thus four times larger in the electrode-shaping geometry. Although the electric field in the ion sheath is also much larger in the electrode-shaping geometry, the time required to quench the discharge is longer due to the highly nonlinear saturation effect of the ionization coefficient at high electric fields.¹⁸ The partial covering of the dielectric layer with charge results in a prolonged discharge in a low electric field regime which favors high efficiency, as mentioned above. In summary, the electrode-shaping geometry [Fig. 1(c)] is more efficient than the standard coplanar-electrode geometry [Fig. 1(a)], because the excitation efficiency is higher in both the cathode ion sheath and the bulk plasma region, and because the more efficient bulk plasma region is wider.

As we noted, the overall duration of the discharge is shorter in the electrode-shaping geometry [Figs. 4(a)–4(d)]. Once the sustain voltage pulse is applied, the time required to reach breakdown is shorter in discharge paths below the outer parts of the sustain electrodes in this structure, due to the larger overvoltage.¹⁹ Thus, the discharges in individual discharge paths in the electrode-shaping geometry initiate earlier but last longer.

C. Dielectric-shaping geometry

In Fig. 1(d), we show a PDP cell with modified shape of the upper dielectric which for brevity will heretofore be referred as the dielectric-shaping geometry. This design was first proposed (without the performance analysis presented here) in Ref. 9 as a way to improve the efficiency of the PDP cell. The dielectric-shaping geometry is characterized by the design parameters a_3 and a_4 . In Fig. 2, we show η and V_{Sm} for the dielectric-shaping geometry with $a_3 = 260 \mu\text{m}$ and $a_4 = 22.5 \mu\text{m}$. All other parameters are the same as in the reference case. We observe that the midmargin voltage V_{Sm} is essentially the same as in the reference case, while the visible light generation efficiency η increases by $\sim 14\%$. As in the electrode-shaping geometry, if a_3 and a_4 are kept constant, and the sustain electrode width w is increased from 300 to $400 \mu\text{m}$, the increase in the visible light generation efficiency η with respect to the reference case is found to be $\sim 17\%$, while once again the operating voltage increases by only a few volts.

The dielectric-shaping geometry [Fig. 1(d)] has an obviously better performance than the standard coplanar-electrode geometry [Fig. 1(a)] and results in larger visible light generation efficiency without substantial increases of

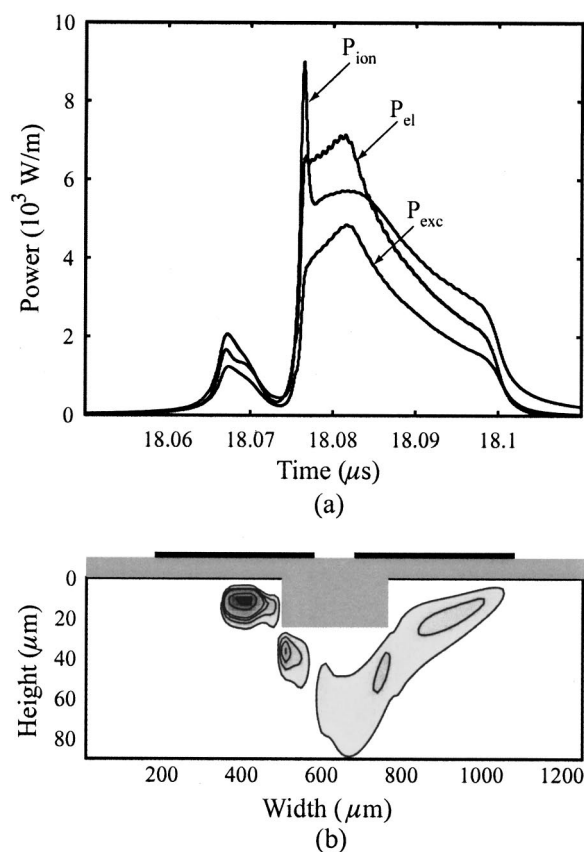


FIG. 6. (a) Dissipated ion power P_{ion} , dissipated electron power P_{el} , and power spent on Xe excitation P_{exc} per unit length for the dielectric-shaping geometry. (b) Normalized power spent for xenon excitation, integrated over a 5 ns time interval, for the dielectric-shaping geometry. The starting time for integration is 80 ns after the beginning of a sustaining period. The increment between the contours and maximum in gray scale are the same as in Figs. 4(c) and 4(d). Note the different vertical scale. Height is measured from the MgO layer surface.

the operating voltages, similar to the electrode-shaping geometry [Fig. 1(c)]. The similar behavior of the two structures could be expected since, in both cases, the modification in cell design basically results in a larger equivalent capacitance of the outer part of the sustain electrodes. We found that the increase in the efficiency without any substantial increase of the operating voltages for the dielectric-shaping geometry can be interpreted in the same way as the improved performance of the electrode-shaping geometry, which was described above in detail. We should nevertheless note two important differences in the performance of these two structures. First, we observe in Fig. 2 that the electrode-shaping geometry has a higher visible light generation efficiency than the dielectric-shaping geometry. Our analyses indicate that η_4 is higher for the electrode-shaping design. The region of high excitation and consequently high UV emission directly below the upper dielectric layer is closer to the phosphor layer in the case of the electrode-shaping design, so that more emitted UV photons reach the phosphor. Second, in Fig. 6(a), we show the dissipated ion power, dissipated electron power, and power spent on Xe excitation in the PDP cell per unit length for the dielectric-shaping geometry. We observe that the peak ionic current is much higher in the dielectric-shaping geometry in comparison with the

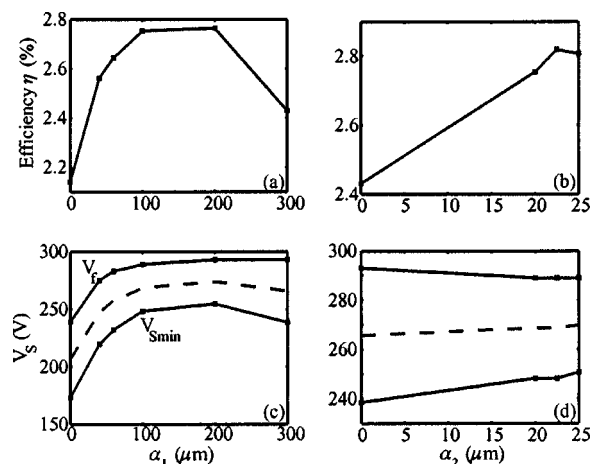


FIG. 7. (a) Visible light generation efficiency η as a function of parameter a_1 of the electrode-shaping geometry for $a_2=20$ μ m [Fig. 1(c)]. All other cell parameters are the same as in the reference case. (b) η as a function of parameter a_2 of the electrode-shaping geometry for $a_1=100$ μ m [Fig. 1(c)]. All other cell parameters are the same as in the reference case. (c) The firing voltage V_f and the minimum sustaining voltage V_{Smin} as a function of a_1 . The dashed line shows the midmargin sustaining voltage V_{Sm} used for the calculation of the efficiency. (d) V_f , V_{Smin} , and V_{Sm} as a function of a_2 .

electrode-shaping geometry. The very large increase in ionic current in the dielectric-shaping geometry is observed when the discharge in the cathode region reaches the point at which the upper dielectric layer length becomes shorter [Fig. 1(d)]. We note that both of the alternative structures are characterized by points of sharp variation of either the electrode shape [Fig. 1(c)] or the upper dielectric shape [Fig. 1(d)]. The electric field is very large in the vicinity of the sharp points as is shown in the equipotential contours in Figs. 3(b) and 3(c) for the electrode-shaping and the dielectric-shaping geometries, respectively. However, in the case of the electrode-shaping geometry, the sharp point is inside the dielectric layer so that the increase in the ionic current in the cathode sheath region is not as dramatic as that observed in the dielectric-shaping geometry. Finally, in Fig. 6(b), we show the normalized power spent for xenon excitation, integrated over a 5 ns time interval, for the dielectric-shaping geometry for comparison with the standard [Fig. 4(c)] and the electrode-shaping geometries [Fig. 4(d)].

D. Dependence of cell performance on design parameters

We now investigate the effect of the design parameters of the PDP cell structures on the visible light generation efficiency and the operating voltages of the PDP cell. Figures 7(a) and 7(c) show the dependence of η , and of V_f , V_{Smin} , and V_{Sm} , respectively, on parameter a_1 of the electrode-shaping geometry [Fig. 1(c)]. We note that $a_1=0$ corresponds to a cell design with the sustain electrodes fully inserted in the upper dielectric layer. As expected, analyses indicate that this design has essentially no difference in performance from a standard coplanar-electrode design [Fig. 1(a)] having the same distance of sustain electrodes from the gap. We also note that $a_1=w$ corresponds to the standard coplanar-electrode design. We observe that as a_1 is increased, both the efficiency and the operating voltages in-

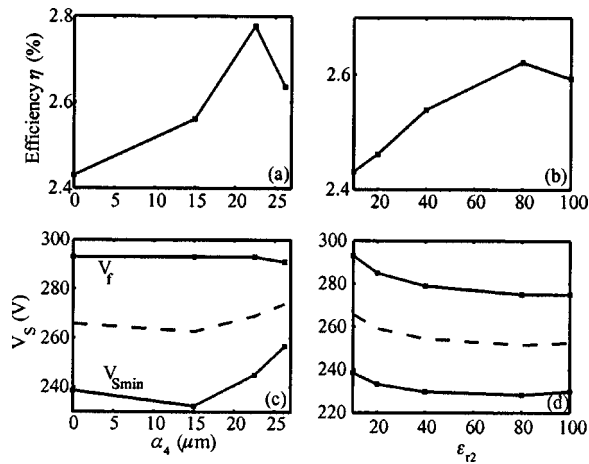


FIG. 8. (a) Visible light generation efficiency η as a function of parameter a_4 of the dielectric-shaping geometry for $a_3=260 \mu\text{m}$ [Fig. 1(d)]. All other cell parameters are the same as in the reference case. (b) η as a function of the dielectric constant ϵ_{r2} of the geometry of Fig. 1(e) for $a_5=200 \mu\text{m}$. All other cell parameters are the same as in the reference case. (c) The firing voltage V_f and the minimum sustaining voltage V_{Smin} as a function of a_4 . The dashed line shows the midmargin sustaining voltage V_{Sm} used for the calculation of the efficiency. (d) V_f , V_{Smin} , and V_{Sm} as a function of ϵ_{r2} .

crease. The efficiency is maximized for $a_1=100 \mu\text{m}$, with any further increases of a_1 leading only to increase in the operating voltages. We conclude that the electrode-shaping geometry has better performance than both the standard coplanar-electrode design [Fig. 1(a)] and the equivalent design with the standard sustain electrodes fully inserted in the upper dielectric layer. In addition, for a specific value of a_2 there appears to be an optimum value of a_1 . In Figs. 7(b) and 7(d), we show the dependence of η , and of V_f , V_{Smin} , and V_{Sm} , respectively, on the parameter a_2 of the electrode-shaping geometry, noting that $a_2=0$ corresponds to the standard coplanar-electrode design. We observe that the visible light generation efficiency of the PDP cell increases substantially as a_2 is increased, while the operating voltages remain essentially the same. The interpretation of the improved performance of this structure [Fig. 1(c)] was discussed in detail in Sec. III B. Figure 7 further shows that the increase in efficiency is maximized for $a_2=22.5 \mu\text{m}$. Analyses indicate that for large values of a_2 , the efficiency of the discharge in heating the electrons η_1 is a decreasing function of a_2 . As a_2 is increased, the electric field in the ion sheath region increases and the sheath length decreases. As a result, the efficiency of the discharge in heating the electrons in the sheath region is a decreasing function of a_2 . This effect dominates for large values of a_2 and results in a decrease of η_1 and subsequently of η .

Figures 8(a)–8(d) show similar results for the dielectric-shaping design and the equivalent design of Fig. 1(e) respectively. The structure of Fig. 1(e) was first proposed (without the performance analysis presented here) in Ref. 9 as a way to improve the efficiency of the PDP cell. The increase of the equivalent capacitance of the outer part of the sustain electrodes in this case is achieved by using a material with a larger dielectric constant ϵ_r in parts of the upper dielectric layer. Figures 8(a) and 8(c) show the dependence of η , and of V_f , V_{Smin} , and V_{Sm} , respectively, on parameter a_4 of the

dielectric-shaping geometry [Fig. 1(d)], while Figs. 8(b) and 8(d) show the dependence of η , and of V_f , V_{Smin} , and V_{Sm} , respectively, on the dielectric constant ϵ_{r2} of the geometry of Fig. 1(e). In both cases, we observe dependences that are similar to those noted for the electrode-shaping geometry. In all three cases, the larger equivalent capacitance of the outer part of the sustain electrodes results in larger visible light generation efficiency of the PDP cell without significant change in the operating voltages. The increase in the efficiency of the device is maximized for a specific value of the corresponding design parameter in each case for reasons described above.

We note that combination of the three different ways of increasing the equivalent capacitance of the outer part of the sustain electrodes does not result in further increase in efficiency. For example, Fig. 7 shows that the efficiency of the electrode-shaping geometry is maximized for $a_2=22.5 \mu\text{m}$. If the equivalent capacitance is further increased by increasing a_2 , the efficiency decreases. We verified that, as expected, if the equivalent capacitance is increased, by either the dielectric-shaping or the dielectric constant methods, the efficiency still decreases.

For the 2D cell geometry variations considered in this article, the electrode shape of the structure of Fig. 1(c) is found to be optimal. For this purpose, we considered alternative shapes of sustain electrodes, for example, a cell design with slanted sustain electrodes.⁸ In such a design, the equivalent capacitance increases linearly with distance rather than sharply as in Fig. 1(c), and results in lower efficiency. The structure of Fig. 1(c) is optimal because it is identical to the standard structure in the middle of the cell [Fig. 1(a)], so that the operating voltages do not change, while in the outer part of the cell, it results in higher equivalent capacitance and higher visible light generation efficiency. We also examined the effect of variations of the lower dielectric layer on the performance of the cell, for example as shown in Fig. 1(f). Such a design results in a wider discharge area and consequently higher excitation efficiency η_{exc} for the reasons described above. However, the overall efficiency η is not larger than the efficiency of the standard structure [Fig. 1(a)]. Analyses indicate that the modification of the lower dielectric layer shape and, consequently, of the phosphor layer shape in the structure of Fig. 1(f) results in lower η_4 . This result could be expected, since most of the visible photons emitted from the vertical sides of the phosphor layer are lost.

IV. SUMMARY

We used a 2D self-consistent simulation model to investigate the performance of several nonstandard plasma display panel cell geometry designs, by focusing our attention on the operating voltages and the visible light generation efficiency of PDP cell designs. The model was used to calculate the voltage margin and the steady-state visible light generation efficiency of PDP cells at their midmargin sustaining voltage. A cell design with a modified shape of sustain electrodes was found to have $\sim 20\%$ larger visible light generation efficiency, without a substantial increase of the operating voltages, when compared to the standard coplanar-electrode de-

sign. A cell design with modified shape of the upper dielectric was found to have $\sim 17\%$ larger visible light generation efficiency, once again without a substantial increase of the operating voltages. A similar performance improvement is achieved by a design involving two different dielectric layers. These geometries are more efficient than the standard coplanar-electrode geometry, because the excitation efficiency is higher in both the cathode ion sheath and the bulk plasma region, and because the more efficient bulk plasma region is wider, due to the increase of the equivalent capacitance of the outer part of the sustain electrodes. A detailed investigation of the dependence of cell performance on the design parameters of these structures indicates that the increase of visible light generation efficiency is maximized for specific values of the corresponding design parameter in each case. Other designs involving alternative shaping of the sustain electrodes or of the lower dielectric layer were found to be less efficient.

ACKNOWLEDGMENTS

This research was supported by the Office of Technology Licensing of Stanford University under Grant No. 127P316 and by the National Science Foundation under Grant No. ATM-9908766.

- ¹A. Sobel, *Sci. Am.* **278**, 70 (1998).
- ²*Electronic Display Devices*, edited by S. Matsumoto (Wiley, New York, 1990), p. 131.
- ³Y. Kanazawa, T. Ueda, S. Kuroki, K. Kariya, and T. Hirose, *SID'99 Digest* (1999), p. 154.
- ⁴Y. Hashimoto, Y. Seo, O. Toyoda, K. Betsui, T. Kosaka, and F. Namiki, *SID'01 Digest* (2001), p. 1328.
- ⁵C. K. Yoon, Y. J. Kim, J. H. Seo, M. S. Yoo, C. B. Park, W. J. Chung, J. H. Yang, K.-W. Whang, and K. C. Choi, *SID'01 Digest* (2001), p. 1332.
- ⁶J. Kang, O. D. Kim, W. G. Jeon, J. W. Song, J. Park, J. R. Lim, and J. P. Boeuf, *IDW'00* (2000), p. 643.
- ⁷G. Oversluizen, S. de Zwart, S. van Heusden, and T. Dekker, *IDW'00* (2000), p. 631.
- ⁸K. J. Shin, J. H. Ryu, and M. H. Park, *SID'99 Digest* (1999), p. 544.
- ⁹C. H. Shon, J. K. Lee, H. C. Kim, S. Dastgeer, S. S. Yang, and S. W. Shin, *SID'01 Digest* (2001), p. 767.
- ¹⁰G. Veronis and U. S. Inan, *J. Appl. Phys.* **91**, 9502 (2002).
- ¹¹W. L. Morgan and B. M. Penetrante, *Comput. Phys. Commun.* **58**, 127 (1990).
- ¹²<http://www.siglo-kinema.com/database/xsect/siglo.sec>
- ¹³J. Meunier, P. Belenguer, and J. P. Boeuf, *J. Appl. Phys.* **78**, 731 (1995).
- ¹⁴S. Rauf and M. J. Kushner, *J. Appl. Phys.* **85**, 3460 (1999).
- ¹⁵T. Shinoda, M. Wakitani, T. Nanto, N. Awaji, and S. Kanagu, *IEEE Trans. Electron Devices* **47**, 77 (2000).
- ¹⁶Y. P. Raizer, *Gas Discharge Physics* (Springer, Berlin, 1997), p. 131.
- ¹⁷C. Punset, S. Cany, and J. P. Boeuf, *J. Appl. Phys.* **86**, 124 (1999).
- ¹⁸Y. P. Raizer, *Gas Discharge Physics* (Springer, Berlin, 1997), p. 57.
- ¹⁹Y. P. Raizer, *Gas Discharge Physics* (Springer, Berlin, 1997), p. 133.